Chemical Science

Accepted Manuscript

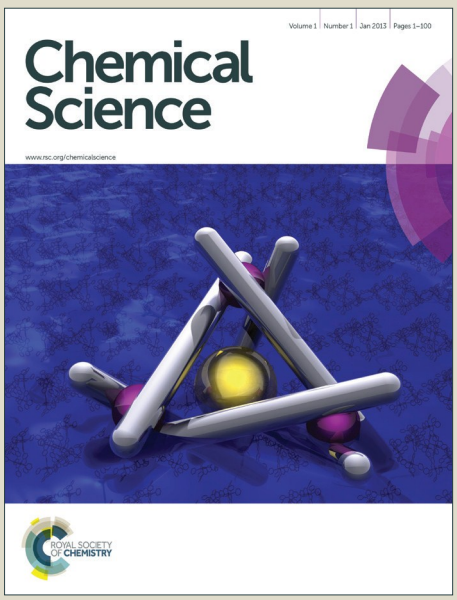

ROYAL SOCIETY OF CHEMISTRY

www.rsc.org/chemicalscience

Cite this: DOI: 10.1039/c0xx00000x

www.rsc.org/xxxxxx

ARTICLE TYPE

A Simple and Effective "Capping" Approach to Readily Tune the Fluorescence of Near-infrared Cyanines

Longwei He,[b] Weiying Lin,*[a,b] Qiuyan Xu,[b] Mingguang Ren,[a] Haipeng Wei,[b] and Jian-Yong Wang[a]

Received (in XXX, XXX) Xth XXXXXXXXX 20XX, Accepted Xth XXXXXXXXX 20XX

DOI: 10.1039/b000000x

Heptamethine cyanines are favorable for fluorescence imaging applications in biological systems owing to their near-infrared (NIR) absorption and emission. However, it is very difficult to quench the fluorescence of NIR dyes by the classic photoinduced electron transfer mechanism due to their relatively high-lying occupied molecular orbital energy levels. Herein, we present a simple and effective "capping" approach to readily tune the fluorescence of NIR cyanines. The resulting new functional NIR dyes **CyBX** (**X** = **O**, **N**, or **S**) not only retain the intact tricarbocyanine scaffold, but also bear a built-in switch to regulate the fluorescence by spiro-cyclization. When compared to traditional cyanines, novel **CyBX** dyes have a superior character in that their NIR optical properties can be readily tuned by the intrinsic spiro-cyclization mechanism. We expect that the "capping" strategy can be extended across not only the visual spectrum and but also to structurally distinct fluorophores.

Introduction

In 1856, Williams first acquired cyanine dyes.[1] The desirable features of cyanine dyes include narrow absorption bands and high molar absorption coefficients. Members of cyanines such as monomethine and trimethine cyanines (Cy3) generally display absorption and emission only in the visible region. The extension of the chromophore backbone of cyanine dyes by one vinylene moiety (CH=CH) may lead to a bathochromic shift by ~100 nm.[2] For instance, the maximal emission wavelengths of pentamethine (Cy5) and heptamethine cyanines (Cy7) can extend well into the near-infrared (NIR) region (> 650 nm). However, increasing length of the polymethine chain may elicit unwanted effects including low fluorescence quantum yields, poor photostability, and aggregation.[3]

With great efforts of the researchers in the field, these limitations have been addressed at least to a certain extent. For example, introduction of a rigid chlorocyclohexenyl ring in the methine chain was employed to improve the stability and the fluorescence quantum yields of cyanine dyes.[4] Maury *et al.* demonstrated that a small, hard anion could polarize the polymethine chain to enhance the stability of cyanines.[5] Blanchard's group reported that conjugation of the cyanine fluorophore Cy5 with a triplet-state quencher could significantly improve the photostability of the dye.[6] Pham and co-workers described that tricarbocyanine modified with four water-soluble sulfonate groups could suppress aggregation.[7]

NIR tricarbocyanine dyes are the most useful members of cyanine dyes and have been applied as functional fluorescent dyes in diverse fields such as monitoring disease biomarkers, detecting biomolecules, monitoring variations of physiological environments, sensing enzyme activity, studying protein-DNA interactions, and evaluating drug efficacy, owing to the pronounced advantages of the NIR properties.[8] Up to date, photoinduced electron transfer (PET) is the main fluorescence mechanism employed for modulating fluorescence of NIR tricarbocyanines (Scheme 1A).[8e-f, 9] However, it is very difficult to quench the fluorescence of NIR dyes by the PET mechanism due to their relatively high-lying occupied molecular orbital (HOMO) energy levels.[10]

This has, for a long time, constrained the full potential applications of this important class of NIR fluorescent dyes. Thus, it is crucial to introduce a new strategy to readily modulate fluorescence of NIR cyanines.

Toward this end, in this contribution, we present a unique means to tune the fluorescence of NIR tricarbocyanines (Scheme 1B). Exemplified by heptamethine cyanine (Cy7), which is a widely used NIR dye, a carboxylic acid moiety (or its amide/thioic derivative) is strategically installed on the carbon 5-position (the central carbon) of the intact cyanine backbone to afford **CyBX**. We envisioned that **CyBX** could transform into **Spiro-CyBX** due to the nucleophilic attack of the heteroatom **X** on the electrophilic carbon 5. As **CyBX** essentially maintains the native scaffold of heptamethine cyanine, like heptamethine cyanine, it should display absorption and emission in the NIR region. However, the typical "push-pull" characteristic of classic cyanines is disrupted in **Spiro-CyBX**, we thus anticipated that **Spiro-CyBX** may show almost no absorption and fluorescence in the NIR region. In other words, the carboxylic acid moiety (or its derivative) may function as a built-in mechanism to readily tune the fluorescence of heptamethine cyanines. Thereby, the transformation of non-fluorescent **Spiro-CyBX** into fluorescent **CyBX** could be exploited to design turn-on type NIR fluorescent probes for bioimaging applications in living systems.

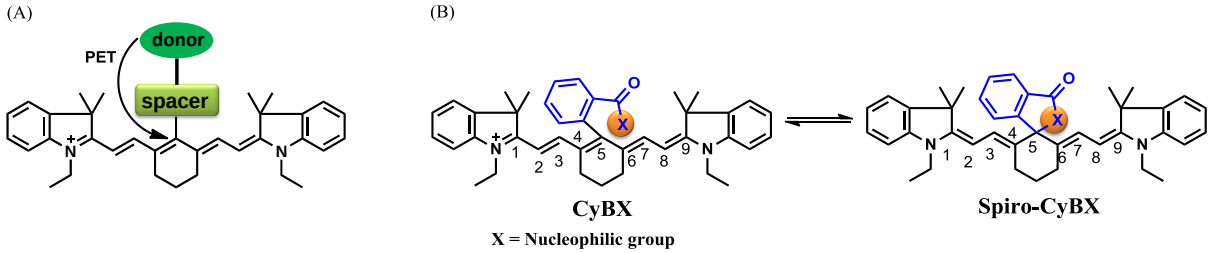

Scheme 1 Design strategy for the new NIR functional dyes **CyBX** (**X = O**, **N**, or **S**) with an intrinsic spirocyclization-based mechanism which modulates fluorescence On-Off. (A) The traditional PET mechanism for tuning fluorescence of heptamethine cyanines. (B) The spirocyclization-based process of the novel functional NIR **CyBX** dyes described in this work.

Herein, we described the rational design, synthesis, and optical properties of the new class of cyanines, **CyBX** NIR functional dyes. We further conducted quantum chemical calculations to shed light on the unique **CyBX** NIR functional dyes. Finally, to demonstrate the potential use of this innovative type of cyanines, we created two turn-on NIR fluorescent probes based on the **Spiro-CyBX** platform for imaging pH changes in living cells and Hg^{2+} in living animals.

Results and discussion

Design and synthesis of CyBX NIR fluorescent dyes

Heteroatoms such as O, N, and S have distinct nucleophilic nature. Thus, their cyclization abilities may significantly vary. Based on the above strategy, we anticipated that **CyBO**, **CyBN**, and **CyBS** compounds (Scheme 2) may have different extents of spirocyclization, which could confer these compounds having diverse optical properties. Thus, we expected that these dyes may be used for different situations in living systems.

The synthesis of compounds **CyBO**, **CyBN**, and **CyBS** is shown in Scheme 1. The starting compounds CyCl and 2-carboxyphenylboric acid in DMF/H_2O were heated under reflux in the presence of $Pd(PPh_3)_4$ to afford **CyBO** *via* the Suzuki-Miyaura method.[11] This synthetic method is very simple with just one step. In addition, it is modular and versatile, as the carboxylic acid could be easily functionalized to afford its various derivatives. For instance, **CyBO** was firstly activated with a standard coupling reagent, N-Hydroxysuccinimide (NHS), followed by reacting with ammonia or sodium sulfide to provide **CyBN** and **CyBS**, respectively. The structures of the products **CyBX** were fully characterized by ^1H NMR, ^{13}C NMR, MS-ESI, and HRMS (ESI†).

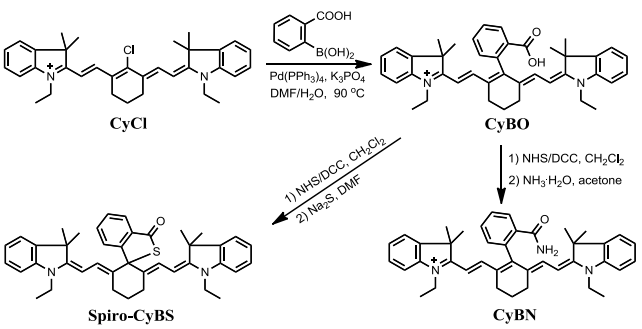

Scheme 2 Synthesis of NIR Functional Dyes **CyBX**.

Optical properties of CyBX NIR fluorescent dyes

The absorption and emission profiles of compounds **CyBX** (**X= O**, **N**, or **S**) in distinct organic solvents (DMF, DMSO, CH_3COCH_3, CH_2Cl_2, MeOH, EtOH, and CH_3CN) are shown in Figures S1-3 (ESI†), and the corresponding photophysical data in DMF are compiled in Table S1 (ESI†). **CyBX** show maximal absorption and emission at around 770 and 800 nm, respectively, which well locate in the NIR region. Notably, as designed, the shapes of absorption/emission spectra of **CyBX** highly resemble those of **CyCl** (Figure S4, ESI†), in good agreement with the fact that **CyBX** dyes keep the same intact cyanine backbone as **CyCl** (Scheme 2). In addition, the photostability of **CyBX** dyes in DMF was measured by continuous irradiation with a Xe lamp (150 W) at 10 nm slit width at the maximal absorption wavelength of **CyBX** dyes. The results demonstrate that less than 6.4% of the initial fluorescence intensity was decreased after 1 hour irradiation (Figure S5), indicating that these NIR dyes have sufficient photostability for potential biological imaging applications.

We then examined the optical properties of the dyes **CyBX** in aqueous solution. As expected, they show drastically differences in absorption intensity in PBS buffer (pH 7.4, 5% DMF) (Figure 1A). The compound **CyBO** exhibits strong absorption at round 770 nm, while **CyBN** has much smaller absorption. By sharp contrast, **CyBS** displays almost no absorption. The visual colors of **CyBX** (0.3 mM, pH = 7.4, PBS/DMF, v/v = 1:1) are consistent with the absorption properties. **CyBO**, **CyBN**, and **CyBS** exhibit green, light green, and pale yellow, respectively (Inset of Figure 1A). **CyBO** is highly fluorescent, while **CyBN** displays good fluorescence, and **CyBS** is essentially non-fluorescent (Figure 1B). Thus, the fluorescence intensity of these dyes is in the order of **CyBO** > **CyBN** > **CyBS,** in accordance with the trend observed in the absorption. These results may be ascribed to the fact that the nucleophilic abilities of heteroatoms are in the order of S > N > O. Thus, the data suggest that in aqueous buffer, for **CyBO**, the ring-opened form (**CyBO**) is predominated; for **CyBN**, the ring-opened form (**CyBN**) and the spiro form (**Spiro-CyBN**) are in equilibrium; for **CyBS**, the spiro form (**Spiro-CyBS**) is essentially predominated.

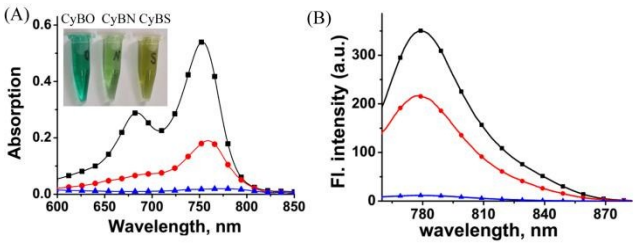

Figure 1 The absorption (A) and fluorescence (B) spectra of the compounds **CyBO** (■), **CyBN** (●), and **CyBS** (▲) (10 μM) in pH = 7.4, PBS/DMF = 95/5. The excitation wavelengths are at 746 nm for **CyBO**, 745 nm for **CyBN,** and 748 nm for **CyBS**, respectively. Inset: (A) The visual color of **CyBX** (left to right: **X = O**, **N**, and **S**.) in PBS aqueous solution.

To support the above hypothesis, we further investigated the fluorescence profiles of the new NIR dyes at different pH values. As shown in Figure 2, **CyBO** shows strong fluorescence over a wide pH range of 4.0-11.0. It is worthy to note that, a gradual drop in the emission with the enhancement of pH is consistent with the hypothesis that the spiro-cyclization ability of the carboxylic acid increases under basic conditions. In the scenario of **CyBN**, a significant decrease of the emission with the increase of pH is observed. This can be explained that the equilibrium of the ring-opened form (**CyBN**) and the spiro form (**Spiro-CyBN**) is shifted to the spiro form (**Spiro-CyBN**) under basic conditions. In the case of **CyBS**, it essentially displays no fluorescence over a wide pH range of 4.0-11.0, implying that even under strong acidic conditions, the spiro form (**Spiro-CyBS**) is still predominated.

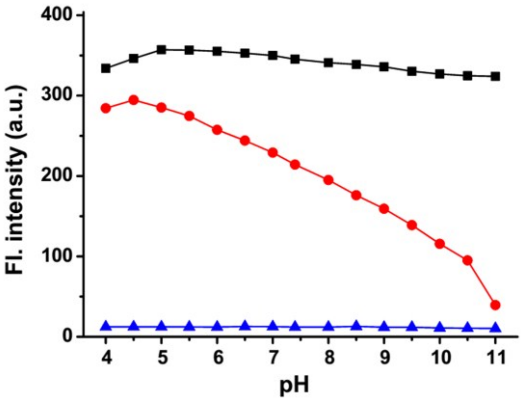

Figure 2 The maximum emission intensity of compounds **CyBO** (■), **CyBN** (●), and **CyBS** (▲) (10 μM, pH = 7.4, PBS/DMF = 95/5) at various pH values. The excitation wavelengths are at 746 nm for **CyBO**, 745 nm for **CyBN**, and 748 nm for **CyBS**, respectively.

To further confirm the design concept, we also compared both the ^{1}H NMR and ^{13}C NMR of **CyBO** and **CyBS,** as these two dyes have different forms predominated. In the case of **CyBO**, the ring-opened form (**CyBO**) is essentially predominated, while for **CyBS**, the spiro form (**Spiro-CyBS**) is predominated. Thus, we should observe a pronounced distinction between **CyBO** and **CyBS** in NMR spectra. Indeed, the chemical shifts of the protons of **CyBS** exhibit a marked shift in respect to those of **CyBO** (Figure 3A). This is consistent with the hypothesis that the spiro-cyclization of **CyBS** leads to the disappearance of the positive charge on the nitrogen, which should confer a strong effect on the chemical shifts of the protons. Importantly, the presence of **CyBS** as the spiro form and **CyBO** as the ring-opened form is clearly evident in ^{13}C NMR spectra. As shown in Figure 3B, the key 5-position carbon of **CyBO** displays a chemical shift at around 140 ppm, in good agreement with its sp^2 character. By sharp contrast, the corresponding 5'-position carbon of **CyBS** has a chemical shift at around 73 ppm, in accordance with its sp^3 character due to the spiro-cyclization.

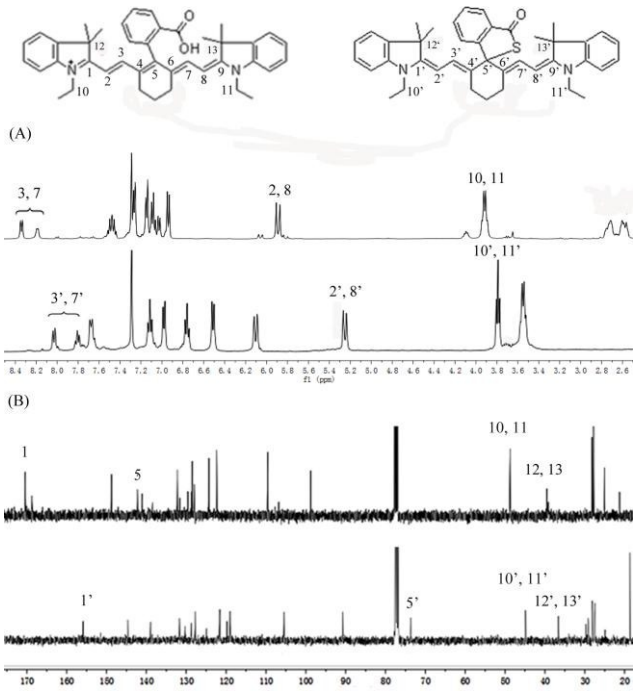

Figure 3 Comparison of partial ^{1}H NMR (A) and ^{13}C NMR (B) spectra of **CyBO** (top) and **CyBS** (bottom) in $CDCl_3$.

Density Functional Theory (DFT) Calculations

To shed light on the optical properties of the new functional NIR fluorescent dyes **CyBX**, DFT calculations with the B3LYP exchange functional employing 6-31G* basis sets using a suite of Gaussian 09 programs were conducted.[12] The frontier molecular orbital plots of **CyBX** are shown in Figure 4. The HOMO−LUMO energy gaps of the dyes are very close, consistent with the above findings that these dyes have similar maximal absorption wavelengths (Table S1, ESI†). Furthermore, the DFT optimized structures of **CyBX** reveal that the benzoic acid (benzamide, or benzothioic acid) moiety is nearly perpendicular to the heptamethine cyanine core (Figure S6 and Table S2, ESI†), indicating that the benzoic acid (benzamide, or benzothioic acid) unit at the *meso*-position has very minor contribution to the π-π conjugated backbone. This is in good agreement with the observation that the benzoic acid (benzamide or benzothioic acid) unit has almost no contribution to the HOMO/LUMO (Figure 6). We then calculated the charge distribution of the optimized structures of **CyBX** by natural bond orbital (NBO) analysis at the B3LYP level (Figure S7, ESI†). The representative atomic charges are displayed in Table S3 (ESI†). 1-, 9-position (C=N) and 5-position (central) carbons exhibit positive charge, while all other carbons on the conjugated backbone show negative charge. However, considering the three-dimensional structures of **CyBX**, only the central (5-position) carbon is likely to be attacked by the nucleophilic heteroatoms atom (O, N, or S) to form the five-membered spiro form (**Spiro-CyBX**).

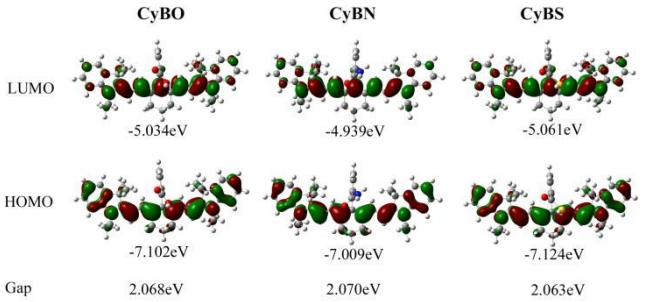

Figure 4 Molecular orbital plots (LUMO and HOMO) and HOMO/LUMO energy gaps of NIR dyes **CyBX** (**X** = **O, N**, or **S**).

Development of an innovative NIR Fluorescent pH Probe for Biological Imaging

The above studies indicate that, like heptamethine cyanine, the new functional NIR dyes **CyBX** have both absorption and emission in the NIR region. Furthermore, importantly, **CyBX** dyes bear an intrinsic fluorescence switch by spiro-cyclization. These highly favorable characters imply that **CyBX** could act as robust platforms for design of NIR fluorescent probes. In addition, the standard MTT assays indicate that **CyBX** have negligible cytotoxicity to living cells (Figure S8, ESI†), suggesting that the new compounds are promising for applications in biological systems. In addition, to investigate the cellular uptake of **CyBX**, we chose **CyBO** as a representative dye for the time-dependent confocal fluorescence imaging of living cells up to 120 min (Figure S9, ESI†). Efficient cellular uptake was observed in the first 30 min of incubation, while the fluorescence was not significantly different after incubating for 30, 60, and 120 min. These data suggest that the cellular uptake of the dye might be *via* endocytosis.[13]

Toward this end, we first tested the possibility of **CyBN** as a novel NIR fluorescent pH probe, as it is sensitive to pH variations as aforementioned (Figure 2). Intracellular pH (pH_i) plays an important role in many biological events including cell proliferation and apoptosis,[14] enzymatic activity,[15] and ion transport.[16] In a typical mammalian cell, the pH_i can vary from 4.7 in lysosome to 8.0 in mitochondria.[17] However, abnormal intracellular pH variations are associated with diseases such as Alzheimer's disease and cancers.[18] Therefore, monitoring pH changes inside living cells is critical for investigating both physiological and pathological processes. So far, a diverse array of fluorescent pH probes have been developed.[8e-g,19] However, only very few of them have both absorption and emission in the NIR region. In addition, most of the reported NIR fluorescent pH probes function by a PET mechanism. By contrast, herein we exploited **CyBN** as a candidate NIR fluorescent pH probe aiming to demonstrate that the internal fluorescence switch by spiro-cyclization in cyanines could effectively be employed for NIR pH probe development (Scheme 3).

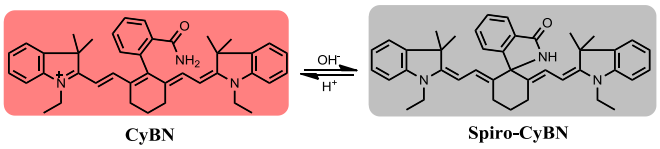

Scheme 3 The ring-opened and spiro form of the NIR probe **CyBN** under acidic and basic conditions.

As shown in Figure 5A, **CyBN** (10 μM, in PBS aqueous containing 5% DMF) displays strong fluorescence at pH 4.5. However, enhancement of pH induces a gradual decrease of emission, in good agreement with the fluorescent images recorded by an *in vivo* imaging system (IVIS Lumina XR (IS1241N6071)) (Figure 5B). The pH-dependence changes in the emission can be rationalized that the fluorescent ring-opened form of **CyBN** dominates under acidic conditions but the non-fluorescent spiro form dominates under basic conditions. The variations in the absorption profiles further support this explanation (Figure S10, ESI†).

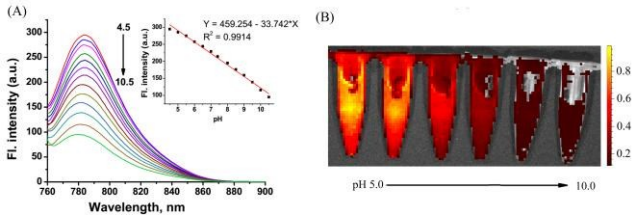

Figure 5 (A) pH-dependence of the fluorescence spectra of the NIR probe **CyBN** (10 μM, PBS/DMF: 95/5) upon excitation at 745 nm. Inset: Plot of the fluorescence intensity versus pH. (B) The fluorescent images of **CyBN** (10 μM, DMF/PBS 5/95) at pH 5.0 to 10.0 using IVIS Lumina XR (IS1241N6071) *in vivo* imaging system with an excitation filter of 675 nm and an emission range of 760-810 nm.

Encouraged by these results, we decided to employ **CyBN** to monitor real-time changes of pH in living cells. Toward this end, EC109 cells were incubated with the probe (5 μM) at 37 ℃ for 30 min, and then the cells were washed with pH 7.0 PBS medium (3 × 1 mL). Upon addition of NH_4Cl, a weak basic reagent that can be used to increase intracellular pH,[20] the variations of the fluorescence intensity of the cells were continuously recorded within 10 minutes (Figures 6 and S11, ESI†). The results indicate that the dye-stained cells display a real-time drop in the emission upon addition of NH_4Cl, which is in good agreement with the pH-dependent changes in fluorescence spectra of **CyBN** in the aqueous solution (Figure 5A).

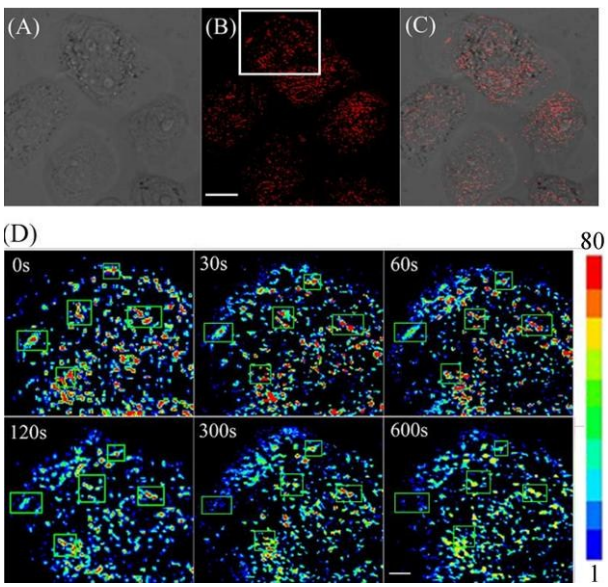

Figure 6 (A) Brightfield image of EC109 cells stained with **CyBN** (5 μM) in pH 7.0 PBS solution. (B) Confocal fluorescence

image of (A). (C) Overlay of (A) and B. (D) Followed by addition of 10 mM NH_4Cl, and then continuously imaged (B) within 10 min. Enlargement of a white box in (B) with *pseudo*color showing the changes of pH with time. The changes of pH were highlighted by green boxes. All images of fluorescence emission were collected between 770 to 810 nm upon excitation at 635 nm. Scale bar = 10 μm for (A)-(C) and 5 μm for (D).

We further investigated the possibility of **CyBN** to visualize endogenous pH changes in an abdominal inflammation model induced by lipopolysaccharides (LPS).[21] Two Kunming rice were intraperitoneally (i.p.) injected with LPS to produce an acute inflammatory response, and one of the mice was then injected with **CyBN**. As shown as in Figure 7, the emission of the mice loaded with both LPS and **CyBN** is stronger than that of the mice incubated with only the probe **CyBN**. As a control, the mice treated with only LPS exhibited almost no fluorescence (Figure 7a). The fluorescent intensity from the abdominal area of the mice was quantified, and the inflamed mice treated with **CyBN** exhibited a higher fluorescence intensity than the normal mice (Figure 7D), which suggests the decrease of the pH value in the inflammatory tissues, consistent with the previous report.[22] Taken together, these results demonstrate that **CyBN** is useful for *in vivo* imaging and can detect the pH changes in small animals.

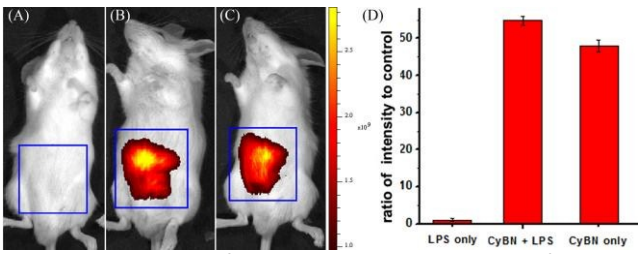

Figure 7 Representative fluorescence images (pseudo-color) of the mice injected with **CyBN** during LPS-mediated inflammatory response *in vivo*. (A) Only LPS was injected as the control. (B) LPS was injected into the peritoneal cavity of the mice, followed by injection with **CyBN** (50 nmol). (C) Only **CyBN** (50 nmol) was injected. (D) Quantification of the emission intensity from the abdominal area of the mice of the experimental groups relative to the control group. All mice were imaged using IVIS Lumina XR (IS1241N6071) *in vivo* imaging system with an excitation filter of 745 nm and an emission range of 760-810 nm.

Development of a new NIR Fluorescent Turn-on Hg^{2+} probe for Biological Imaging in Living Animals

The thiol-affinity to Hg^{2+} has been exploited to construct fluorescent probes for mercury cation.[23] **CyBS** contains a strong nucleophilic benzothioate and shows almost no fluorescence as the spiro form (**Spiro-CyBS**) dominates. Thus, we envisioned that, upon reaction with Hg^{2+}, the thiol moiety of non-fluorescent **Spiro-CyBS** may coordinate with Hg^{2+} to result in formation of the highly fluorescent **CyBS-Hg-CyBS** (Scheme 4). In other words, **CyBS** may exhibit a fluorescence-enhanced signal in the presence of Hg^{2+}.

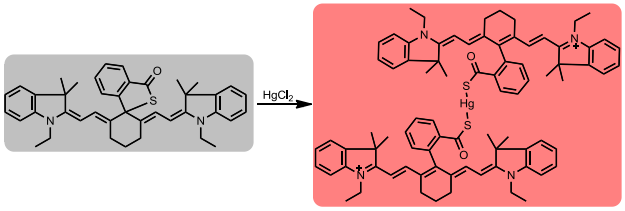

Scheme 4 The likely sensing mechanism of **CyBS** with Hg^{2+}.

As designed, the free probe **CyBS** is almost non-fluorescent in PBS solution (pH 7.4, 30% MeOH). However, addition of Hg^{2+} ions elicits a dramatic effect on both the fluorescence and absorption spectra (Figures 8A and S12, ESI†). A significant fluorescence turn-on response is observed due to the Hg^{2+}-mediated formation of the opened form, and the detection limit was calculated to be 7.27×10^{-7} M (S/N = 3) (Figure S13, ESI†). Mass spectrometry analysis confirms that the probe coordinates with Hg^{2+} to form a fluorescent ring-opened form of **CyBS-Hg-CyBS** (Figure S14, ESI†), which is consistent with the sensing mechanism reported for benzothioate-based fluorescent Hg^{2+} probes.[23] Furthermore, as displayed in Figure 8B, the probe is highly selective to Hg^{2+} over other various relevant metal ions (K^+, Na^+, Ca^{2+}, Mg^{2+}, Ag^+, Al^{3+}, Cr^{3+}, Fe^{3+}, Ni^{2+}, Cu^{2+}, Zn^{2+}, and Cd^{2+}) and reactive oxygen species (ROS) including HClO and H_2O_2.

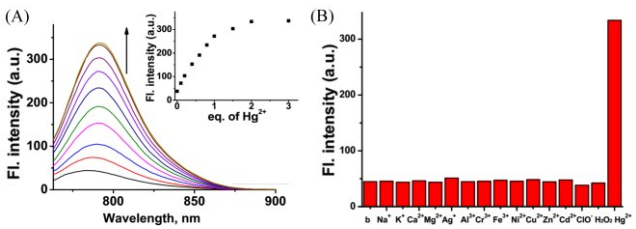

Figure 8 (A) Fluorescence spectra of **CyBS** (10 μM) in the presence of various concentrations of Hg^{2+} (0–30 μM) in phosphate buffer (pH 7.4, 30 % MeOH) with excitation at 745 nm. Inset: Fluorescence intensity of **CyBS** at 745 nm vs Hg^{2+} concentration (0-3 equivalents). (B) Fluorescence intensity at 792 nm of **CyBS** (10 μM) with excitation at 745 nm in the presence of various species, such as 200 equivalents of K^+, Na^+, Ca^{2+}, and Mg^{2+}; 20 equivalents of Ag^+, Al^{3+}, Cr^{3+}, Fe^{3+}, Ni^{2+}, Cu^{2+}, Zn^{2+}, and Cd^{2+}; 2 equivalents of ClO^-, H_2O_2, and Hg^{2+}.

We proceeded to evaluate the ability of the probe to function in living cells. EC109 cells incubated with **CyBS** (5 μM) for 30 min at 37 ℃ provide almost no fluorescence (Figure 9B). By contrast, the cells incubated with the probe and then Hg^{2+} give strong fluorescence (Figure 9D). These results demonstrate that **CyBS** is cell membrane permeable and can respond to Hg^{2+} with a turn-on signal in the living cells.

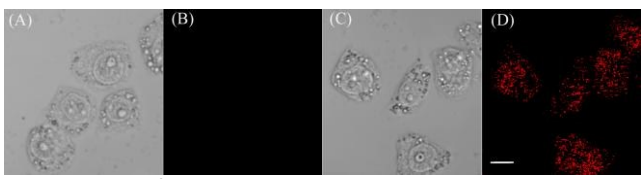

Figure 9 Images of EC109 cells treated with the probe **CyBS** in the absence or presence of Hg^{2+}. (A) Brightfield image of EC109 cells incubated with only **CyBS** (5 μM) for 30 min; (B) fluorescence image of (A); (C) Brightfield image of EC109 cells incubated with **CyBS** (5 μM) for 30 min and further treated with Hg^{2+} (5 μM) for another 5 min; and (D) Fluorescence image of (C).

Fluorescent images (B) and (D) were collected between 770 to 810 nm upon excitation at 635 nm. Scale bar = 10 μm.

To further demonstrate the potential of the probe for imaging applications in living animals owing to its advantageous NIR absorption and emission, the probe was treated with the mice in the absence or presence of Hg^{2+} ions. As shown in Figure 10B, the control Kunming mice i.p. injected with only **CyBS** (50 nmol) provide very weak fluorescence. However, followed by i.p. injection with Hg^{2+} (100 nmol) at the same site, a significant increase of fluorescence intensity is noted (Figures 10C and 10D). These results are in good agreement with the data aforementioned in aqueous solution (Figure 8A) and living cells (Figure 9). Taken together, these studies indicate that the new NIR probe **CyBS** can image Hg^{2+} not only in the living cells but also in living animals, demonstrating its value.

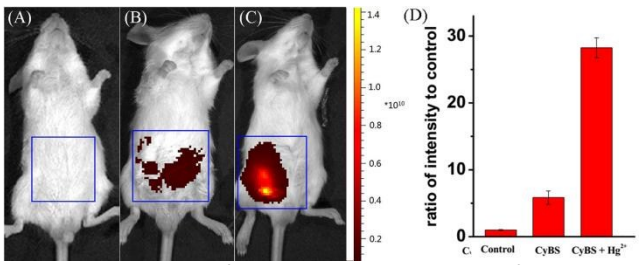

Figure 10 Representative fluorescent images (*pseudo*color) of the mice. (A) Fluorescent image of the negative control, neither **CyBS** nor Hg^{2+} is injected; (B) Fluorescent image of the mice treated with only **CyBS** (50 nmol) for 10 min; (C) Fluorescent image of the mice injected with **CyBS** (50 nmol) for 10 min, followed by an i.p. injection of Hg^{2+} (100 nmol); (D) Quantification of the emission intensity from the abdominal area of the mice of the experimental groups relative to the control group. All mice were imaged using IVIS Lumina XR (IS1241N6071) *in vivo* imaging system with an excitation filter of 745 nm and an emission range of 760-810 nm.

Conclusions

In summary, we introduced the simple and effective capping approach to readily tune the fluorescence of NIR cyanines. The unique strategy is based on direct installation of a benzoic acid (benzamide, or benzothioic acid) moiety into the intact cyanine backbone. The resulting new functional NIR dyes **CyBX** (**X** = **O**, **N**, or **S**) not only retain the intact tricarbocyanine scaffold, but also bear a built-in switch to regulate the fluorescence by spiro-cyclization. Thus, like traditional NIR cyanines, **CyBX** exhibit both absorption and emission in the NIR region. Furthermore, importantly, **CyBX** dyes display a unique nature; their NIR optical properties can be readily tuned by the intrinsic spiro-cyclization mechanism. To our best knowledge, such type of NIR cyanines is unprecedented. We further showed that **CyBN** could be employed to monitor real-time pH changes in living systems and **CyBS** could be used to detect Hg^{2+} in both living cells and living animals with a turn-on signal, demonstrating the values of the NIR functional fluorescent dyes **CyBX**. We expect that the capping strategy can be extended across not only the visual spectrum and but also to structurally distinct fluorophore species. More broadly, the findings described herein suggest the possible development of a series of next-generation functional dyes with optical profiles that are readily tunable. A diverse array of optical probes with such exciting properties would likely find widespread application as powerful molecular tools in studies involved in fluorescence microscopy.

Acknowledgment

Funding was partially provided by NSFC (21172063, 21472067) and the startup fund of University of Jinan.

Notes and references

[a] *Institute of Fluorescent Probes for Biological Imaging, School of Chemistry and Chemical Engineering, School of Biological Science and Technology, University of Jinan, Jinan, Shandong 250022, P.R. China. E-mail: weiyinglin2013@163.com*

[b] *State Key Laboratory of Chemo/Biosensing and Chemometrics, College of Chemistry and Chemical Engineering, Hunan University, Changsha, Hunan 410082, P. R. China.*

† Electronic Supplementary Information (ESI) available: [Experimental procedures, characterization data, and additional spectra]. See DOI: 10.1039/b000000x/

1. C. H. G. Williams, *Trans.–R. Soc. Edinburg*, 1856, **21**, 377.
2. V. W. KÖnig, *Angew. Chem.*, 1925, **38**, 743.
3. R. P. Haughland, Molecular probes. Handbook of fluorescent probes and research chemicals, Molecular Probes Inc, Eugene, OR, 9th edn, 2002.
4. L. Strekowski, Heterocyclic polymethine dyes: synthesis, properties and applications; Springer, Berlin/Heidelberg, 2008.
5. P.-A. Bouit, C. Aronica, L. Toupet, B. L. Guennic, C. Andraud and O. Maury, *J. Am. Chem. Soc.*, 2010, **132**, 4328.
6. R. B. Altman, D. S. Terry, Z. Zhou, Q. Zheng, P. Geggier, R. A. Kolster, Y. Zhao, J. A. Javitch, J. D. Warren and S. C. Blanchard, *Nat. Methods*, 2012, **9**, 68.
7. W. Pham, L. Cassell, A. Gillman, D. Koktysh and J. C. Gore, *Chem. Commun.*, 2008, **18**, 1895.
8. (a) W. M. Leevy, S. T. Gammon, H. Jiang, J. R. Johnson, D. J. Maxwell, E. N. Jackson, M. Marquez, D. Piwnica-Worms and B. D. Smith, *J. Am. Chem. Soc.*, 2006, **128**, 16476; (b) Y. Liu, M. Chen, T. Cao, Y. Sun, C. Li, Q. Liu, T. Yang, L. Yao, W. Feng and F. Li, *J. Am. Chem. Soc.*, 2013, **135**, 9869; (c) K. Pu, A. J. Shuhendler and J. Rao, *Angew. Chem. Int. Ed.*, 2013, **52**, 10325; (d) K. Kundu, S. F. Knight, N. Willett, S. Lee, W. R. Taylor and N. Murthy, *Angew. Chem. Int. Ed.*, 2009, **48**, 299; (e) B. Tang, F. Yu, P. Li, L. Tong, X. Duan, T. Xie and X. Wang, *J. Am. Chem. Soc.*, 2009, **131**, 3016; (f) R. Tang, H. Lee and S. Achilefu, *J. Am. Chem. Soc.*, 2012, **134**, 4545; (g) X. Peng, F. Song, E. Lu, Y. Wang, W. Zhou, J. Fan and Y. Gao, *J. Am. Chem. Soc.*, 2005, **127**, 4107; (h) S. A. Hilderbrand, K. A. Kelly, M. Niedre and R. Weissleder, *Bioconjugate Chem.*, 2008, **19**, 1635; (i) X. Li, W. Shi, S. Chen, J. Jia, H. Ma and O. S. Wolfbeis, *Chem. Commun.*, 2010, **46**, 2560; (j) M. Whitney, E. N. Savariar, B. Friedman, R. A. Levin, J. L. Crisp, H. L. Glasgow, R. Lefkowitz, S. R. Adams, P. Steinbach, N. Nashi, Q. T. Nguyen and R. Y. Tsien, *Angew. Chem. Int. Ed.*, 2013, **52**, 325; (k) S. Zhang, V. Metelev, D. Tabatadze, P. C. Zamecnik and A. J. Bogdanov, *Proc. Natl. Acad. Sci. U.S.A.*, 2008, **105**, 4156; (l) Z. Yang, J. H. Lee, H. M. Jeon, J. H. Han, N. Park, Y. He, H. Lee, K. S. Hong, C. Kang and J. S. Kim, *J. Am. Chem. Soc.*, 2013, **135**, 11657.
9. (a) X. Wang, L. Cui, N. Zhou, W. Zhu, R. Wang, X. Qian and Y. Xu, *Chem. Sci.*, 2013, **4**, 2936; (b) S.-Y. Lim, K.-H. Hong, D. I. Kim, H. Kwon and H.-J. Kim, *J. Am. Chem. Soc.*, 2014, **136**, 7018; (c) K. Xu, M. Qiang, W. Gao, R. Su, N. Li, Y. Gao, Y. Xie, F. Kong and B. Tang, *Chem. Sci.*, 2013, **4**, 1079.
10. (a) D. Rehm and A. Weller, *Isr. J. Chem.*, 1970, **8**, 259; (b) T. Egawa, K. Hanaoka, Y. Koide, S. Ujita, N. Takahashi, Y. Ikegaya, N. Matsuki, T. Terai, T. Ueno, T. Komatsu and T. Nagano, *J. Am. Chem. Soc.*, 2011, **133**, 14157.
11. H. Lee, J. C. Mason and S. Achilefu, *J. Org. Chem.*, 2006, **71**, 7862.
12. M. J. Frisch *et al.*, GAUSSIAN 09 (Revision A.02), Gaussian, Inc.: Pittsburgh, PA, 2009.
13. Chunbai He, Kuangda Lu and Wenbin Lin, *J. Am. Chem. Soc.*, 2015, **136**, 12253.

14. (a) R. A. Gottlieb, H. A. Giesing, J. Y. Zhu, R. L. Engler and B. M. Babior, *Proc. Natl. Acad. Sci. U.S.A.*, 1995, **92**, 5965; (b) R. A. Gottlieb and A. Dosanjh, *Proc. Natl. Acad. Sci. U.S.A.*, 1996, **93**, 3587.
15. R. T. Kennedy, L. Huang and C. A. Aspinwall, *J. Am. Chem. Soc.* 1996, **118**, 1795.
16. (a) P. Donoso, M. Beltran and C. Hidalgo, *Biochemistry* 1996, **35**, 13419-13425; (c) R. G. W. Anderson and L. Orci, *J. Cell Biol*. 1988, **106**, 539.
17. S. Chen, Y. Hong, Y. Liu, J. Liu, C. W. T. Leung, M. Li, R. T. K. Kwok, E. Zhao, J. W. Y. Lam, Y. Yu and B. Z. Tang, *J. Am. Chem. Soc.*, 2013, **135**, 4926
18. (a) H. Izumi, T. Torigoe, H. Ishiguchi, H. Uramoto, Y. Yoshida, M. Tanabe, T. Ise, T. Murakami, T. Yoshida, M. Nomoto and K. Kohno, *Cancer Treat. Rev.*, 2003, **29**, 541; (b) R. J. Gillies, N. Raghunand, M. L. Garcia-Martin and R. A. Gatenby, *IEEE Eng. Med. Biol. Mag.*, 2004, 57.
19. (a) J. Han and K. Burgess, *Chem. Rev.*, 2010, **110**, 2709; (b) Q. Wan, S. Chen, W. Shi, L. Li and H. Ma, *Angew. Chem. Int. Ed.*, 2014, **53**, 10916; (c) J. Han, A. Loudet, R. Barhoumi, R. C. Burghardt and K. Burgess, *J. Am. Chem. Soc.*, 2009, **131**, 1642; (c) G. Li, D. Zhu, L. Xue and H. Jiang, *Org. Lett.*, 2013, **15**, 5020; (d) A. M. Dennis, W. J. Rhee, D. Sotto, S. N. Dublin, G. Bao, *ACS Nano*, 2012, **6**, 2917.
20. (a) A. Roos and W. F. Boron, *Physiol. Rev.*, 1981, **61**, 296; (b) M. Tantama, Y. P. Hung and G. Yellen, *J. Am. Chem. Soc.*, 2011, **133**, 10034.
21. (a) P. Li, H. Xiao, Y. Cheng, W. Zhang, F. Huang, W. Zhang, H. Wang and B. Tang, *Chem. Commun.*, 2014, **50**, 7184; (b) M. S. Trent, C. M. Stead, A. X. Tran and J. A. Hankins, *J. Endotoxin Res.*, 2006, **12**, 205.
22. (a) A. Lardner, *J. Leukocyte Biol.*, 2001, **69**, 522; (b) F. Okajima, *Cell. Signalling*, 2013, **25**, 2263; (c) S. Schreml, R. J. Meier, O. S. Wolfbeis, M. Landthaler, R.-M. Szeimies and P. Babilas, *Proc. Natl. Acad. Sci. U.S.A.*, 2011, **108**, 2432.
23. (a) W. Shi and H. Ma, *Chem. Commun.*, 2008, 1856; (b) X.-Q. Zhan, Z.-H. Qian, H. Zheng, B.-Y. Su, Z. Lan and J.-G. Xu, *Chem. Commun.*, 2008, 1859.